

Combining EPR spectroscopy and X-ray crystallography to elucidate the structure and dynamics of conformationally constrained spin labels in T4 lysozyme single crystals

Philipp Consentius¹, Ulrich Gohlke², Bernhard Loll³, Claudia Alings³, Udo Heinemann^{2,1}, Markus C. Wahl^{3,5}, Thomas Risse^{1,4,*}

¹ Freie Universität Berlin, Institute of Chemistry and Biochemistry, Takustr. 3, 14195 Berlin, Germany

² Medicine in the Helmholtz Association, Robert-Rössle-Str. 10, 13125 Berlin, Germany

³ Freie Universität Berlin, Institute of Chemistry and Biochemistry, Laboratory of Structural Biochemistry, Takustr. 6, 14195 Berlin, Germany

⁴ Berlin Joint EPR Laboratory Freie Universität Berlin

⁵ Helmholtz-Zentrum Berlin für Materialien und Energie, Macromolecular Crystallography, Albert-Einstein-Straße 15, D-12489 Berlin, Germany

Abstract:

Electron paramagnetic resonance (EPR) spectroscopy in combination with site-directed spin labeling is used to investigate the structure and dynamics of conformationally constrained spin labels in T4 lysozyme single crystals. Within a single crystal, the oriented ensemble of spin bearing moieties results in a strong angle dependence of the EPR spectra. A quantitative description of the EPR spectra require the determination of the unit cell orientation with respect to the sample tube and the orientation of the spin bearing moieties within the crystal lattice. Angle dependent EPR spectra were analyzed by line shape simulations using the stochastic Liouville equation approach developed by Freed and co-workers and an effective Hamiltonian approach. The gain in spectral information obtained from EPR spectra of single crystalline samples taken at different frequencies namely X-band and Q-band allows to discriminate between motional models describing the spectra of isotropic solutions similarly well. In addition, it is shown that angle dependent single crystal spectra allow to identify two spin label rotamers with very similar side chain dynamics. These results demonstrate the utility of single crystal EPR spectroscopy in combination with spectral line shape simulation techniques to extract valuable dynamic information not readily available from the analysis of isotropic systems. In addition, it will be shown that the loss of electron density in high resolution diffraction experiments at room temperature does not allow to conclude that there is significant structural disorder in the system.

Introduction

Site-directed spin labeling (SDSL) combined with an electron paramagnetic resonance (EPR) characterization of the labeled entities has become a versatile tool in biophysics.¹⁻⁶ A selected residue is specifically labeled with a paramagnetic probe. In case of proteins molecular biology techniques are used to replace the native amino acid typically into a cysteine, which allows specific attachment of spin labels e.g. using a sulfhydryl reactive nitroxide radical (Figure S1). SDSL has become popular as it is a sensitive technique requiring only few tens of picomoles of labeled molecules without restrictions with respect to correlation times. This in turn allows to apply the technique to large systems such as membrane proteins or macromolecular complexes. A suite of SDSL techniques have been developed to investigate macromolecular structure and dynamics. The characterization of distance distribution between two spin labels using pulsed dipolar spectroscopy (DEER or PELDOR) has become very popular in recent years as it provides quantitative excess to distance distributions up to several nanometers.⁷⁻⁹ Pulsed dipolar spectroscopy on nitroxides requires low temperature, which limits its ability to probe the dynamics of the systems. Among other methods, analyzing the line shape of CW spectra provides information about the dynamics of the systems.^{1, 10, 11} The analysis utilizes the anisotropic interaction of the nitroxide with the external magnetic field. A detailed analysis requires information about the structure of the spin-labeled side chain as well as its dynamics. In solution or suspension such an analysis is not straightforward. However, it has been shown that additional information can be obtained from analyzing ordered systems.¹²⁻¹⁴

Within this study, we want to show that the analysis of spin-labeled protein single crystals allows to gain additional information, not readily available from the analysis of isotropic systems. In particular, we want to combine EPR spectroscopy with structural analysis of the system by X-ray crystallography focusing on conformationally restricted sites in T4 lysozyme. In addition, to a discussion of the experimental framework, which allows to extract structural as well as dynamic

information of the system, we want to compare X-ray crystallography and EPR spectroscopy at room temperature to exemplify the complementarity of the methods.

Results and Discussion

CW EPR-spectra of conformationally restricted spin labels in T4 lysozyme single crystals show a strong angle dependence, which allows to obtain structural and dynamic information of the spin label.^{15, 16} However, an analysis of the single crystal EPR spectra without additional information about the orientation of the unit cell with respect to the magnetic field turned out to be challenging due to the space group of T4 lysozyme crystals exhibiting six molecules in the unit cell. Therefore, the orientation of the crystal unit cell within the EPR sample tube is a prerequisite for a detailed analysis of the EPR spectra. Experimentally this was approached by mounting a spin-labeled T4 lysozyme single crystal into a quartz capillary and measuring an angle dependent series of CW EPR spectra. The spectrum obtained for variant 118R1 (s. Figure S1 and S3) taken at a reference orientation of the capillary with respect to the external magnetic field called 0° is shown in Figure 1A. The cartesian EPR laboratory frame is defined with its z-axis being aligned with the external magnetic field and the x-axis chosen to be along the long capillary axis (Figure 1B), which is the rotation axis for the angle dependent experiments. The orientation of the T4 lysozyme crystal with respect to the quartz capillary was determined by tagging the capillary to identify the reference orientation and mounting it onto the goniometer head of an X-ray diffractometer. The reference orientation was aligned with the direction of the x-ray beam (Figure 1C). From the positions of the Bragg peaks taken for some angles of incident the unit cell parameters as well as the orientation of the unit cell in space were determined. For spin-labeled T4 lysozyme single crystals the data revealed a trigonal crystal system in space group P3₂21 with six symmetry related protein molecules in line with previous investigations.¹⁷⁻

¹⁹ Unit cell parameters were found to be $a=b=60\text{\AA}$, $c=97\text{\AA}$ with associated angles of $\alpha=\beta=90^\circ$ and $\gamma=120^\circ$.

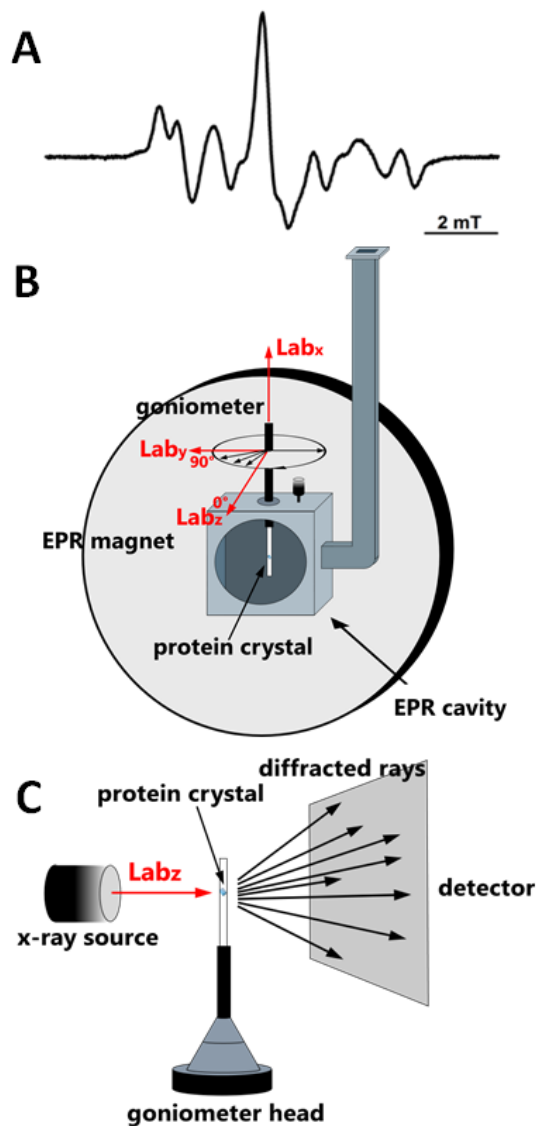


Figure 1. Experimental setup to study protein single crystals using X-ray diffraction and EPR spectroscopy. A) EPR spectrum of a spin-labeled 118R1 T4L single crystal at a reference (0°) orientation of the magnetic field. B) definition of the EPR laboratory coordinate system; the z-axis of this coordinate system is aligned with the static magnetic field. C) The orientation of the crystallographic unit cell within the capillary is determined at the given reference orientation using short dose X-ray diffraction.

While these two experiments are in principle sufficient to allow for an analysis of the angle dependent EPR spectra, it is important to take a set of EPR data after the determination of the crystal orientation. On the one hand, subsequent EPR experiments show that the X-ray dose was sufficiently low to keep the reducible nitroxide in its paramagnetic state. On the other hand, these experiments are important to ensure that the local environment of the spin probe as well as the position of the crystal in the quartz capillary are not changed. As shown in Figure 2A, the superposition of the two EPR spectra reveals only small variations of the line shape in terms of amplitude and peak positions, which excludes significant changes of the crystal orientation as well as the local environment. While the low field region of both spectra is identical, the small differences observed at high fields can be explained by the reproducibility of the sample alignment, which induces an uncertainty of a few degrees. To further illustrate the impact of line shape variation upon crystal rotation in more detail, the 0° reference measurement (black line, Figure 2A) is superimposed by two EPR spectra obtained by either a $+10^\circ$ (red line, middle panel) or a -10° (red line, bottom panel) rotation around the capillary x-axis. Strong variations in the high field region, especially observed for amplitude and peak positions emphasize the sensitivity upon slight variations regarding the magnetic field direction.

A suspension of micro crystals at 298 K shows a spectral width of 7.03 mT (Figure S2), which is consistent with a nitroxide side chain exhibiting a fast but conformationally restricted motion.¹⁷

¹⁸ For the spectra taken at 0° and -10° a spectral width of 6.5 and 6.9 mT is found, respectively, indicating that some of the spin labels are oriented almost perfectly along the π -orbital of the nitroxide for the latter spectrum. The strong variations of the EPR line shape upon crystal rotation supports a well-defined orientation of the spin bearing moiety with respect to the magnetic field, which is in line with a motion of the spin label side restricted in amplitude but rather high frequency as inferred from the line shape of the microcrystal suspension.^{16, 18}

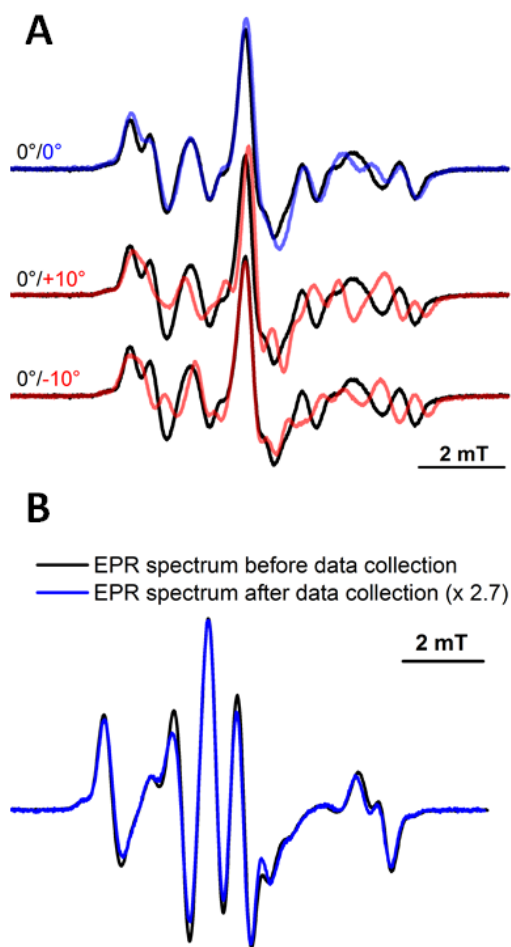


Figure 2. EPR spectra of a spin-labeled 118R1 T4L single crystal. A) EPR spectrum measured at the 0° reference orientation of the magnetic field before (black) and after unit cell determination (blue, top). The variations of spectral line shape upon capillary rotation of +10° (red, middle panel) and -10° (red, bottom panel) are superimposed by the 0° reference measurement (black). B) Two EPR spectra of the protein crystal were obtained before the acquisition of a full X-ray diffraction data set (black line) and afterwards (blue line, spectrum was multiplied by 2.7).

A quantitative description of the angle resolved EPR spectra of protein single crystals requires – in addition to the orientation of the crystal lattice in the laboratory framework discussed above – information about the orientation of the spin bearing moiety within the crystal lattice. To this end, X-ray crystallography is used, which is typically performed at low temperature to avoid modification of the system due to radiation damage. High resolution structures of variant 118R1

obtained at 100 K allow to identify a conformation of the spin label, which results in an unfolding of the short helix F to accommodate the spin label conformation (Figure S3).^{15, 16, 18} The data obtained at 1.0 Å resolution (pdb entry 5JDT) allows to identify a water molecule residing between the nitroxide and the carbonyl moiety of residue G107 to contribute to the stabilization of the conformation by hydrogen bonding (Figure S3).¹⁶

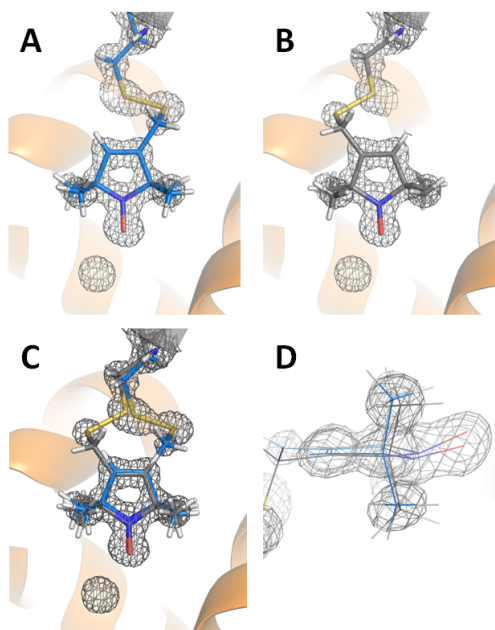


Figure 3. Structural model of the two L118R1 side chain conformers in a stick representation superimposed by a 2Fo-Fc density difference map ($\sigma = 1.5$) obtained at 100 K. The two rotameric states of T4L 118R1 are shown in A and B in top view. A superposition of the two states is shown either in a stick representation (top view, C) or lines representation (D, side view).

A detailed inspection of the high-resolution electron density reveals that the well-resolved electron density of the nitroxide ring is not due to a single conformation of the spin label side chain. As shown in Figure 3 two conformations of the disulfide linkage with equal population are required to describe the electron density and to obtain a good R-factor. It is surprising that both conformation result in an almost perfect superposition of the nitroxide rings. To this end it is worth mentioning that the nitroxide ring is bent in both conformations. As the nitroxide ring is

rotated by 180° if going from one to the other conformation this observation clearly suggests that the bent conformation is induced by the environment. This is in line with theoretical calculations showing that the potential energy surface is very flat along the bending coordinate of the ring.¹⁵ A likely reason for the observed bending here is the stabilization of the spin label conformation by the hydrogen bonding discussed above (s. Figure S3). The two side chain models provide information about the dihedral angles of the two spin label rotamers, which can be assigned using the convention proposed by Lovell et al.²⁰ A multitude of X-ray crystallographic studies of nitroxide spin labels demonstrate that the {m,m}-conformation, comprising dihedral angles of $X1 = 300^\circ$ and $X2 = 300^\circ$, is the most abundant conformation found for spin-labeled side chains engineered at solvent exposed α -helical sites (e.g. ^{17, 19, 21}). For the two spin label conformations discussed here, the first dihedral angle ($X1$) was measured to be either $X1 = 248^\circ$ (Figure 3A) or $X1 = 254^\circ$ (Figure 3B). Significant deviations with respect to the energetically relaxed {m,m}-conformation ($X = 300^\circ$) of $X1$ indicate that some energy is required to accommodate the spin label into this conformation. The second dihedral angle ($X2$) was measured to be $X2 = 46^\circ$ (Figure 3A) or $X2 = 164^\circ$ (Figure 3B), which are rather close to the {t}-conformation ($X = 180^\circ$) and {p}-conformation ($X = 60^\circ$). Neither {m,t} nor {m,p}-rotamers were observed for solvent exposed R1 side chains as steric clashes involving the S_δ sulfur atom were predicted.²² These observations demonstrate an energetic unfavorable configuration of the first two dihedral angles ($X1/X2$) of the spin label side chain as compared to solvent exposed helical sites. The disulfide bridge, whose rotation is defined by the dihedral angle $X3$ can adopt two conformations of either $X3 \sim 90^\circ$ or $X3 \sim 270^\circ$, which was also found for solvent exposed spin-labeled side chains.^{13, 22} The interconversion of the two rotameric states is separated by a barrier of about 28 – 38 kJ/mol,²³⁻²⁵ which results in characteristic time scales for the interconversion being long compared to the EPR time scale. Hence the two conformations can be considered static and result in two spectral contributions to the EPR line shape. The structural model of the two R1 conformers depicted in Figure 3C reveals a $X3$ dihedral angle of either $X3 \sim 75^\circ$ or $X3 \sim 267^\circ$,

which is almost in line with the expected values for a low energy conformation.²³⁻²⁵ This analysis suggests that part of the stabilization of the observed conformation by both, the packing of the surrounding protein side chains as well as the energetic contribution of the hydrogen bonding effects of the nitroxide via a water molecule to the adjacent carbonyl moiety of Glycine 107 (s. Figure S23), is used to allow for the unfavorable $X1$ and $X2$ dihedral angles. The presence of two conformations gives rise to some heterogeneity in the sample, which has impact on the simulation of EPR spectra discussed below.

The structural results obtained at low temperature may be misleading in case the system obeys a different or more than one conformation at room temperature. For variant 118R1 of T4 lysozyme it has recently been shown that X-ray diffraction at room temperature (PDB entry 5G27) allows to identify a second conformation of the protein in the crystal, which is absent at cryogenic temperature.¹⁶ The angle resolved EPR spectra are fully consistent with the structural information from diffraction. In addition, EPR spectroscopy allows to prove that both conformations are in thermodynamic equilibrium.¹⁶ It is well known that prolonged X-ray exposure at room temperature can induce electron induced processes, which may modify the system. In particular, the disulfide bridge may be cleaved or electron induced reduction the nitroxide may occur. Thus, it needs to be ensured that the disulfide bridge of the spin label side chain as well as the spin label environment is not modified by X-ray diffraction performed at room temperature. Figure 2B shows the superposition of the EPR spectrum obtained before (black trace) and after (blue trace, multiplied by factor 2.7) the X-ray diffraction experiment. While the intensity of the EPR spectra drops to about 1/3 of the initial value, the line shape is not changed by prolonged X-ray exposure. In light of the very nice agreement between the angle resolved EPR spectra and the structure of the spin labels by X-ray diffraction, this result provides strong evidence for the integrity of the spin label side chain as well as its local environment upon X-ray exposure.¹⁶ The spin probe is, however, reduced to a significant fraction. While the

reduction does not affect the orientation of the spin label in the two conformations, it does influence their relative stability. This effect can be rationalized by the fact that the conformation observed at low temperature is stabilized by hydrogen bonding of a water molecule in the lattice between the oxygen of the nitroxide and the carbonyl carbon of residue G107. Reduction to the hydroxylamine will alter the hydrogen bonding and hence the relative stability of the conformers.¹⁶

The reproducibility as well as the internal consistency of the approach was verified by comparing angle dependent measurements of two different spin-labeled single crystals of variant 118R1. For two differently oriented, isomorphous single crystals, the two planes probed by rotation of the crystal will intersect in one line resulting in the necessity that two spectra with appropriate orientation of the magnetic field have to be identical. EPR data of two crystals were measured in 10° steps each. For the two crystals, the magnetic field is oriented in two different planes of the Cartesian crystal frame as shown in Figure 4A. From the orientation of the crystal lattice a counterclockwise rotation of the two crystals with respect to the reference orientation by 77° and 124° , respectively, was inferred from diffraction to result in the same orientation of the magnetic field with respect to the crystal lattice. Hence, spectra measured at 80° and 120° , which were the closest to the theoretical values, respectively are shown in Figure 4B. The line shape is very similar. The differences observed in both cases are in line with expectations due to the slight misalignment compared to the ideal situation.

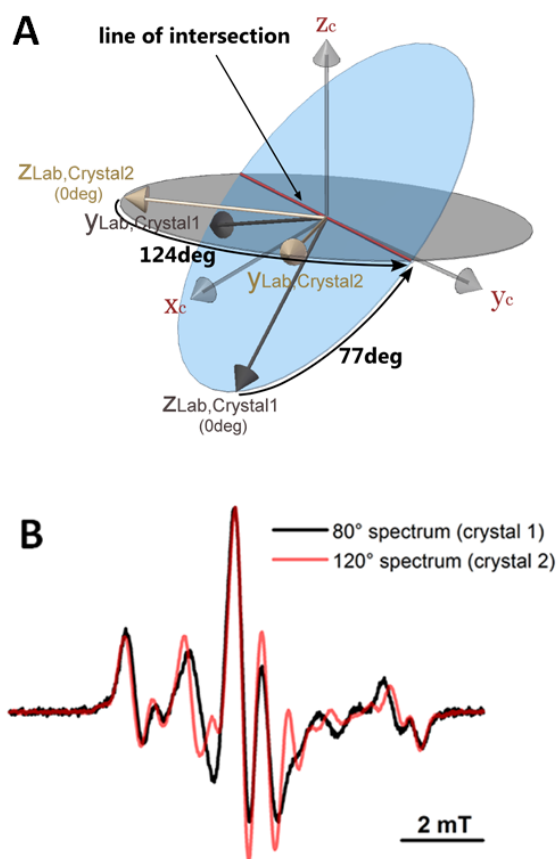


Figure 4. A) The gray shaded coordinate system (x_c , y_c , z_c) defines the Cartesian crystal frame of the unit cell for two different crystals. The blue and gray planes represent the 10° step wise measurements of the two EPR laboratory frames. The $Z_{\text{Lab,Crystal1}}$ -axis represents the direction along the external magnetic field of the first crystal (0°) and $Y_{\text{Lab,Crystal1}}$ the axis being perpendicular with respect to the magnetic field. $Z_{\text{Lab,Crystal2}}$ and $Y_{\text{Lab,Crystal2}}$ define the parallel and perpendicular axes for the second crystal. The 77° measurement of the first crystal and the 124° measurement of the second crystal are predicted along the line of intersection. The EPR spectra of the measurement taken at 80° (black trace, crystal 1) and 120° (red trace, crystal 2) are shown in B.

Comparison of motional models to describe spin label dynamics

The theoretical description of the EPR line shape is a powerful technique to extract detailed information on the internal dynamics of the spin bearing moiety.^{15, 26} To eliminate global tumbling effects of the protein in solution, the sample is commonly recorded either in a 30 %

sucrose solution^{27, 28} or immobilized by using attachment to a surface by complexation or covalent attachment.^{29, 30} The internal dynamics of the R1 side chain is commonly considered to be characterized by rotations around the five dihedral angles X_1 - X_5 (Figure S4). From a number of studies it was inferred that the rotation around the first three dihedral angles do not contribute to the rotational dynamics observed in EPR.^{17, 19, 22} Therefore, the so-called X_4/X_5 -model, which identifies the two terminal bonds as the ones contributing most to the spin label dynamics, was put forward to describe the rotational motion of solvent exposed helical sites.^{13, 26} The line shape of EPR spectra obtained from proteins labeled at solvent exposed helical sites could be simulated using a framework developed by the Freed group, which allows to describe the rotational dynamics of the spin label by diffusion in an ordered potential.^{31, 32} As terminal bonds are not oriented along the direction of the principal components of the g- and hyperfine tensors, the tilt angle $\beta_D=36^\circ$ between the molecular nitroxide frame (Z_M) and the rotational diffusion frame (Z_R) (see Figure 5A) obtained from the best fits are in line with this model.(e.g.^{13, 31, 32} While the motion of the spin label variant 118R1 is much more restricted it is still possible that librational motion around the terminal bond contribute to its dynamics. The X-Band EPR spectrum obtained from a suspension of microcrystals is characteristic of a fast motion of spin label with small amplitude as discussed above.¹⁶ Figure 5B shows the best fit to this spectrum using the so-called MOMD model^{31, 32} for the director of the potential aligned with the z-axis of the magnetic tensors (red trace) or tilted by 36° (blue trace).

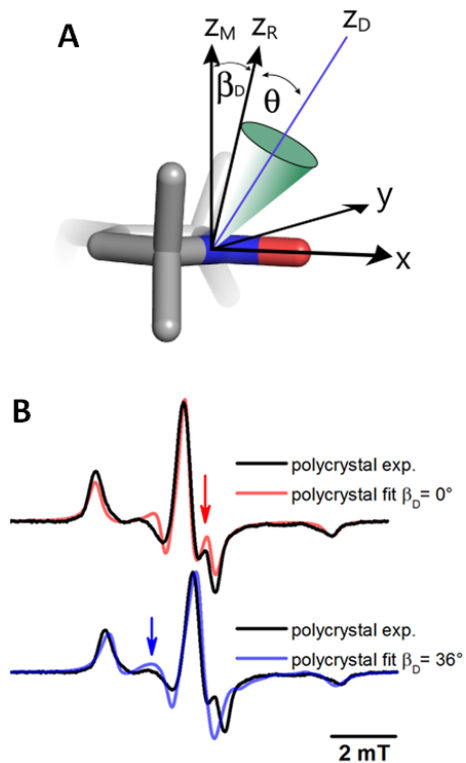


Figure 5. A) Molecular model of the nitroxide group of a spin-labeled R1 side chain, which is used to describe the z-axis anisotropic motion. In this convention, z_M is defined as the molecular z-axis being related to the rotational diffusion frame (z_R) by the angle β_D . The uniaxial director frame z_D is the symmetry axis of the restoring potential which is related to the diffusion frame by the angle θ . B) X-Band EPR spectrum of a suspension of T4L microcrystals of variant 118R1 (black). EPR line shape fits were performed using the stochastic Liouville approach by Freed with either a collinear alignment of the director frame and the nitroxide tensor frame (red trace) or a tilted arrangement with $\beta_D=36^\circ$ (blue trace). Both fits were performed using an order parameter of $S=0.9$ and values in the range of 8.0-8.5 for $\log R_{xx}$, $\log R_{yy}$, and $\log R_{zz}$, respectively.

Both fits show noticeable deviations from the experimental spectrum, however, the fit obtained for $\beta_D=36^\circ$ fails to resolve the g-tensor anisotropy observed on the high field side of the central line, which renders this model less likely to be correct. To further discriminate between the two models, angle-dependent single crystal EPR spectra of T4 lysozyme variant 118R1 were evaluated using the same approach. The spectral line shape simulations were performed using

the orientation of the unit cell with respect to the magnetic field determined by X-ray diffraction and the orientation of the magnetic tensors was taken from the two conformations found by X-ray diffraction at room temperature.¹⁶ Figure 6A shows two single crystal EPR spectra (black traces) taken at a magnetic field orientation of 0° and 90°, respectively. The line shape simulation for each magnetic field orientation was performed using different values of β_D superimposed as red traces in Figure 6A. For both crystal orientations, a collinear alignment of the director frame and the nitroxide tensor frame results in an accurate description of all spectral features in the single crystal EPR spectra (Figure 6A) as long as the angle β_D is chosen to be 0°. The ratio of the two spin label conformations was set to 75:25, which is in line regarding earlier studies of this spin-labeled lysozyme variant.¹⁶ The observed deviations in signal amplitude and line widths can be explained by the simplified Brownian motional model, which assumes an axial symmetry of potential restricting the dynamics of the spin bearing moiety. In addition, only a single rotamer of the major spin label conformation (Figure 3A) is used to simulate the single crystal line shape. This in turn neglects the structural heterogeneity introduced by the second rotameric state of the spin label found at low temperature. Introducing a tilt of the director frame with respect to the g- and hfi-matrices ($\beta_D=5^\circ$, $\beta_D=10^\circ$ or $\beta_D=36^\circ$) (Figure 6A) results in significant deviation of the simulations from the experiments. From these results, it is readily clear that the experimental data is inconsistent with a motional model in which the director of the potential is not aligned with the z-axis of the magnetic tensors (Figure 6A).

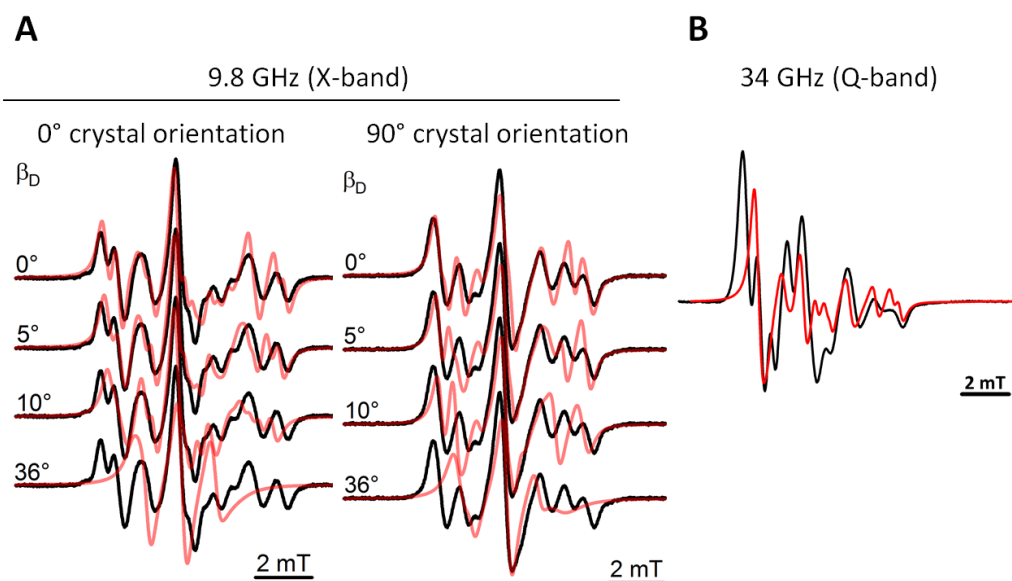


Figure 6. Single crystal EPR spectra with corresponding line shape simulations obtained at X-band (A) and Q-band (B). A) Two EPR spectra of the spin-labeled 118R1 single crystal were performed having the external magnetic field being oriented in a 0° or 90° angle. Line shape simulations were performed using different tilt angles of the director frame with respect to the magnetic tensor frame in red ($\beta_D = 0^\circ, 5^\circ, 10^\circ$ or 36°). B) Single crystal EPR spectrum of T4L 118R1 obtained at Q-band (black) is superimposed by a line shape simulation using $\beta_D = 0^\circ$.

A critical test for the accuracy of the model is its ability to describe spectra taken at different microwave frequencies (e.g. ³³). To this end, Figure 6B shows exemplarily one spectrum out of an angle dependent series taken at 34 GHz (Q-band) of a 118R1 T4 lysozyme single crystal. The simulation shown in red is based on the same model assumptions used to successfully fit the X-band data. The quality of the fit is significantly deteriorated as compared to X-band. This is associated with contributions of the g-tensor anisotropy of the g_{xx} and g_{yy} present in the low field region of the spectrum, which is averaged in the model used here. In contrast, the high field region where the A_{zz}/g_{zz} components dominate, the EPR line shape can be described in a reasonably well as far as peak positions are concerned.

The internal dynamics of the 118R1 nitroxide moiety is characterized by rotational motion in the ns-range, which allows to describe the result of the restricted amplitudes of motion by an effective Hamiltonian approach.³⁴ EPR spectrum of a suspension of microcrystals of T4L variant 118R1 taken at X-band (black trace, Figure 7A) can be fitted reasonably well using the effective Hamiltonian approach (red trace), even though it is not significantly better than the fit using a $\beta_D = 0^\circ$ shown in Figure 5B. The best-fit values (see Table S2) were further used to simulate EPR spectra of a T4L 118R1 single crystal of known orientation at X-band and Q-band. The effective Hamiltonian model can describe the As shown in the angle dependent single crystal EPR spectra (X-band) of T4 lysozyme variant 118R1 with similar fidelity as the stochastic Liouville approach (Figure 7B) assuming the same ratio of 75:25 for the two spin label conformations. Deviations in signal amplitude and especially in line widths can be explained by the simplistic dynamic model, which empirically introduces Lorentzian lines of constant width for all resonances. Interestingly, the single crystal EPR spectrum obtained at Q-band (Figure 7C, black trace) can be simulated comparably well using the same set of magnetic parameters and the aforementioned ratio of the two conformers (Figure 7C, red). Both, the spectral features in the high field region, where the A_{zz}/g_{zz} components dominate the EPR line shape, as well as the motional g_{xx} and g_{yy} contributions, which are resolved in the low field region are described reasonably well. Please note that fits of equal quality are found for the entire angle dependent series (see Figure S5 for additional examples). Please note that additional spectral information available from the angle dependent measurements allows to judge the validity of motional models, which is very difficult based on spectra performed on isotropic samples only.

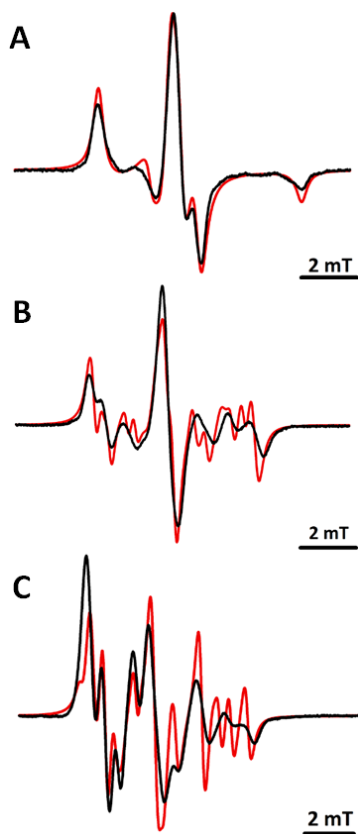


Figure 7. A) X-Band EPR spectrum of a polycrystalline suspension of the spin-labeled T4L 118R1 variant (black) superimposed by a line shape simulation using the effective Hamiltonian approach. B) Single crystal EPR spectra of T4L 118R1 obtained at X-band (B, black) or Q-band (C, black) superimposed by a line shape simulation using the effective Hamiltonian approach (red).

Structure of 115/119RX Spin-labeled T4 Lysozyme determined at 298 K

The discussion of the EPR results obtained from single crystals of T4 lysozyme variant 118R1 given above was nicely supported by the structure obtained by X-ray diffraction, which identified two spin label conformations at room temperature. However, most X-ray structures of spin-labeled protein single crystals the spin bearing nitroxide is not resolved. This is typically interpreted as disorder of the side chain, which cannot be further evaluated based on the diffraction results. The structure of T4 lysozyme variant 115/119RX, in which the spin label is tethered to two cysteine residues (see Figure S1), was determined at 100 K and exhibits a well-resolved electron density of the nitroxide ring (pdb entry: 3L2X and 5LWO).^{15, 17} It was previously shown that angle resolved single crystal EPR spectra taken at room temperature can

be understood based on this structure.¹⁵ The room-temperature structure of the T4 lysozyme variant 115/119RX was solved by X-ray diffraction at a resolution of 1.8 Å and deposited in the Protein Data Bank (pdb entry: 5NXO). Figure 8A shows the 115/119RX spin label side chain (gray sticks) attached to the short α -helix G shown in ribbon representation. The $2F_o-F_c$ electron density map of the RX side chain (blue mesh) obtained at room temperature is restricted to the two Sulphur atoms of both tethers, which allows to model a single spin label conformation whose orientation is chosen to minimize the angular constraints of the bidentate tether.

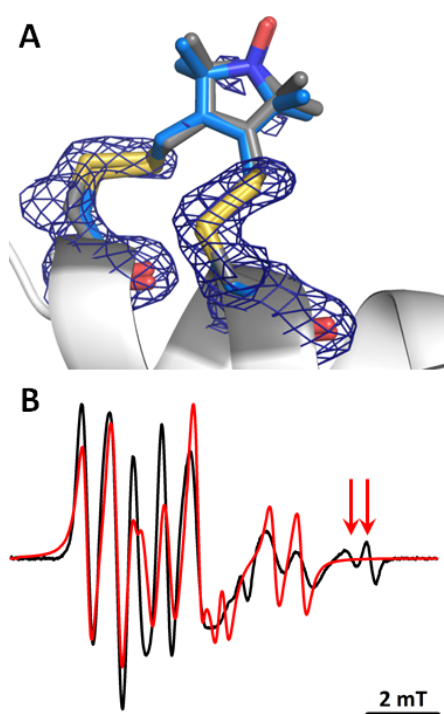


Figure 8. Crystal structure of T4L 115/119RX with a corresponding single crystal EPR spectrum. A) The crystal structure of the T4L 115/119RX variant was obtained at room-temperature and refined to a resolution of 1.8 Å. The RX side chain model (shown in stick representation, gray) is superimposed by a $2F_o-F_c$ density difference map contoured at $\sigma = 1.0$ (blue mesh). The RX side chain of the 115/119RX crystal structure determined at 100 K (PDB entry: 5LWO) is superimposed in blue. B) EPR spectrum of a T4L 115/119RX spin-labeled single crystal obtained at 34 GHz (black) superimposed by a line shape simulation using the effective Hamiltonian approach for a single spin label conformation (red).

In contrast to the low temperature structure (PDB entry: 5LWO), the electron density of the unsaturated five-membered 3-pyrroline-*N*-oxide ring is not resolved, which is typically explained by structural heterogeneity at room temperature. However, a superposition of the two RX side chain models obtained at either 100 K (Figure 8A, blue sticks) or 298 K (gray sticks) are almost coincident having atomic deviations of less than 1 Å for all atoms. This observation suggests that the degree of disorder that leads to the loss of resolved electron density of the nitroxide ring is not particularly high. To elucidate this point further it is interesting to compare the results obtained from X-ray crystallography with single crystal EPR spectra. Figure 8B shows an EPR spectrum taken at Q-band of a spin-labeled T4 lysozyme single crystal variant 115/119RX (black trace). The angle dependent series of spectra show a significant variation of the line shape within the series (Figure S6), which rules out the presence of an isotropic contribution. The spectral line shape simulations for this variant were performed using the same framework, which was successfully applied to describe the dynamics of the T4L variant 118R1. (for details on the values of the *g*- and *hfi*-matrices for see Table S3). As shown in Figure 8B (red trace), the line shape simulation based on the atomic positions of the room temperature conformation is suitable to describe the majority of spectral features in the Q-band spectrum reasonably well. As mentioned earlier, apparent deviations in signal amplitude and line widths are due to the simplistic effective Hamiltonian model. A striking difference between the experimental data and the theoretical simulation is found in the high-field region of the spectrum, where two additional spectral features (marked with arrows) are not described by the model discussed above. The two lines have similar amplitude, which is considerably smaller than the one of the other lines observed in the spectrum. This suggests that these might originate from a minority conformation of the spin label. Evidence for such a conformation may be found in the electron density. A close inspection reveals additional electron density patches, which cannot be assigned to atoms of the major conformation discussed above. As indicated in Figure 9A these can be assigned to Sulphur atoms of a second RX conformer (arrow). To this end, it is interesting to note that a similar

fragmented electron density around the RX side chain was also found at 100 K.¹⁵ The structural model based on the low temperature data is superimposed in orange to the electron density obtained at room temperature. It is seen that the green electron density patch can be explained by the Sulphur atom of the conformation adapted from the second RX conformation obtained at low temperature (orange sticks).

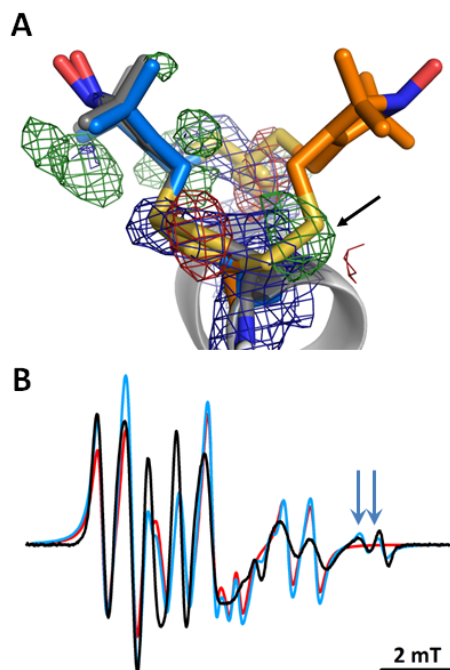


Figure 9. Crystal structure of T4L 115/119RX with a corresponding single crystal EPR spectrum. A) The crystal structure of the T4L 115/119RX variant was obtained at room-temperature and refined to a resolution of 1.8 Å. The RX side chain model (shown in stick representation, gray) is superimposed by a $2F_o-F_c$ density difference map contoured at $\sigma = 1.0$ (blue mesh) and a F_oF_c map contoured to either $\sigma = +3.0$ (green mesh) or $\sigma = -3.0$ (red mesh). Additionally, the two 115/119RX side chain conformers determined at 100 K (PDB entry: 5LWO) are superimposed in blue (major conformation) and orange (minor conformation). The arrow points to an additional electron density patch, which could not be assigned by the room temperature model. B) EPR spectrum of a T4L 115/119RX spin-labeled single crystal obtained at 34 GHz (black). Line shape simulations were performed using either a single spin label conformation (red) or the two spin label conformations obtained at low temperature (blue).

Adding the second spin label conformation to the model used to simulate the EPR line shape simulations results in the blue trace shown in Figure 9B. The best fit (blue trace) was found for a ratio of the two conformations of 85:15 (85 % for the main conformation). It is clearly seen that adding the second conformation is capable to describe the spectral components not captured by the single component fit (red trace). It is important to note that the dynamics of the side chains in both conformers is very similar (we used the same set of effective magnetic parameters, see Table S3), which renders an identification based on CW EPR experiments of isotropic samples impossible. However, the two conformers and their exchange dynamics may play an important role to understand the complex spin physics observed in such system. Finally, we want to stress that EPR spectroscopy provide solid evidence for a well-defined orientation of the spin bearing moieties despite the fact that X-ray crystallography lacks a resolved electron density of the nitroxide. This highlights the complementarity of the two methods in particular if systems exhibiting internal dynamics are considered.

In summary, the present study aims at analyzing structural as well as dynamic properties of conformationally constrained spin labels in T4 lysozyme single crystals. The crystallization of spin-labeled variants of T4 lysozyme results in a well-defined orientation of the spin bearing moieties within the crystal lattice. Single crystal EPR spectra of these samples are strongly angle dependent, which boosts the amount of spectroscopic information compared to the solution spectrum and allows to gain additional information such as the presence of more than one spin label conformation with similar rotational dynamics. In this context, we provide a general experimental framework for analyzing the EPR line shape of spin-labeled protein single crystals, which uses X-ray diffraction to determine the orientation of the unit cell with respect to the magnetic field. Furthermore, X-ray crystallography at room temperature is explored to extract the structural properties of the spin label at comparable conditions as used for EPR spectroscopy. Due to the internal dynamics of the protein at room temperature, structural information on the

nitroxide ring may be difficult to achieve because of a lack of resolved electron density even for conformationally restrained spin labels such as the RX side chain. However, the EPR spectroscopic results clearly suggest that the spin label has a rather well-defined orientation in space and the line shape analysis allows to confirm the structural model inferred from the observed electron density. The spectral resolution available for the single crystals allows to evaluate different theoretical models used to simulate the line shape of CW EPR spectra. For the highly constrained side chains considered here, we could show that at X-band both the stochastic Liouville approach^{31, 32} as well as the effective Hamiltonian approach³⁴ are suitable theoretical models analyzing angle dependent EPR spectra obtained from spin-labeled protein single crystals. From a molecular point of view, the ability of the stochastic Liouville approach to describe the spectrum is surprising as it assumes a rotational average of the x and y direction of the nitroxide tensor, which is implausible. The fundamental weakness becomes immediately obvious if spectra are taken at higher frequency (shown here for Q-band), which increases the spectral anisotropy due to the Zeeman interaction. Hence, at Q-band (34 GHz) the spectra can only be described by the effective Hamiltonian approach, confirming the model of a small amplitude motion around every axis.

Acknowledgement

T.R. acknowledge support by the cluster of excellence (314) Unifying Concepts in Catalysis (UniCat) funded by the DFG and hosted at the Technische Universität Berlin. The molecular biology part of this study was done in the molecular biophysics laboratory of the Department of Physics of FU Berlin. We acknowledge access to beamline BL14.3 of the BESSY II storage ring (Berlin, Germany) *via* the Joint Berlin MX-Laboratory funded by the Helmholtz Zentrum Berlin für Materialien und Energie, the Freie Universität Berlin, the Humboldt-Universität zu Berlin, the Max-Delbrück Centrum für Molekulare Medizin, and the Leibniz-Institut für Molekulare Pharmakologie.

References

1. D. S. Cafiso, *Acc. Chem. Res.*, 2014, 47, 3102-3109.
2. G. E. Fanucci and D. S. Cafiso, *Curr. Opin. Struct. Biol.*, 2006, 16, 644-653.
3. W. L. Hubbell, C. J. López, C. Altenbach and Z. Yang, *Curr. Opin. Struct. Biol.*, 2013, 23, 725-733.
4. J. P. Klare, *J. Biol. Chem.*, 2013, 394, 1281-1300.
5. I. D. Sahu, R. M. McCarrick and G. A. Lorigan, *Biochemistry*, 2013, 52, 5967-5984.
6. N. Van Eps, L. N. Caro, T. Morizumi and O. P. Ernst, *Photochem. Photobiol. Sci.*, 2015, 14, 1586-1597.
7. H. S. Mchaourab, P. R. Steed and K. Kazmier, *Structure*, 2011, 19, 1549-1561.
8. G. Jeschke, *Annu. Rev. Phys. Chem.*, 2012, 63, 419-446.
9. G. Jeschke and Y. Polyhach, *Phys. Chem. Chem. Phys.*, 2007, 9, 1895-1910.
10. L. Columbus and W. L. Hubbell, *Trends Biochem. Sci.*, 2002, 27, 288-295.
11. W. L. Hubbell, A. Gross, R. Langen and M. A. Lietzow, *Curr. Opin. Struct. Biol.*, 1998, 8, 649-656.
12. B. P. Binder, S. Cornea, A. R. Thompson, R. J. Moen and D. D. Thomas, *Proc. Natl. Acad. Sci. U S A.*, 2015, 112, 7972-7977.
13. K. Jacobsen, S. Oga, W. L. Hubbell and T. Risse, *Biophys. J.*, 2005, 88, 4351-4365.
14. T. Risse, W. L. Hubbell, J. M. Isas and H. T. Haigler, *Phys. Rev. Lett.*, 2003, 91, 188101.
15. P. Consentius, B. Loll, U. Gohlke, C. Alings, C. Müller, R. Müller, C. Teutloff, U. Heinemann, M. Kaupp and M. C. Wahl, *J. Phys. Chem. Lett.*, 2017, 8, 1113-1117.
16. P. Consentius, U. Gohlke, B. Loll, C. Alings, R. Müller, U. Heinemann, M. Kaupp, M. Wahl and T. Risse, *J. Am. Chem. Soc.*, 2016, 138, 12868-12875.

17. M. R. Fleissner, M. D. Bridges, E. K. Brooks, D. Cascio, T. Kalai, K. Hideg and W. L. Hubbell, *Proc. Natl. Acad. Sci. U S A.*, 2011, 108, 16241-16246.
18. Z. Guo, D. Cascio, K. Hideg, T. Kalai and W. L. Hubbell, *Protein Sci.*, 2007, 16, 1069-1086.
19. R. Langen, K. J. Oh, D. Cascio and W. L. Hubbell, *Biochemistry*, 2000, 39, 8396-8405.
20. S. C. Lovell, J. M. Word, J. S. Richardson and D. C. Richardson, *Proteins*, 2000, 40, 389-408.
21. M. A. Lietzow and W. L. Hubbell, *Biochemistry*, 2004, 43, 3137-3151.
22. M. R. Fleissner, D. Cascio and W. L. Hubbell, *Protein Sci.*, 2009, 18, 893-908.
23. D. B. Boyd, *J. Am. Chem. Soc.*, 1972, 94, 8799-8804.
24. R. R. Fraser, G. Boussard, J. K. Saunders, J. B. Lambert and C. E. Mixan, *J. Am. Chem. Soc.*, 1971, 93, 3822-3823.
25. D. Jiao, M. Barfield, J. E. Combariza and V. J. Hruby, *J. Am. Chem. Soc.*, 1992, 114, 3639-3643.
26. L. Columbus, T. Kalai, J. Jeko, K. Hideg and W. L. Hubbell, *Biochemistry*, 2001, 40, 3828-3846.
27. H. S. McHaourab, M. A. Lietzow, K. Hideg and W. L. Hubbell, *Biochemistry*, 1996, 35, 7692-7704.
28. R. Langen, K. Cai, C. Altenbach, H. G. Khorana and W. L. Hubbell, *Biochemistry*, 1999, 38, 7918-7924.
29. K. Jacobsen, S. Oga, W. L. Hubbell and T. Risse, *Biophys. J.*, 2005, 88, 4351-4365.
30. C. J. López, M. R. Fleissner, Z. Guo, A. K. Kusnetzow and W. L. Hubbell, *Protein Sci.*, 2009, 18, 1637-1652.
31. D. E. Budil, S. Lee, S. Saxena and J. H. Freed, *J. Magn. Reson.*, 1996, 120, 155-189.

32. D. J. Schneider, and J. H. Freed., in *Spin Labeling Theory and Applications*, ed. L. J. R. Berliner, J., New York, NY, 1989, pp. 1–76.
33. J. P. Barnes, Z. Liang, H. S. Mchaourab, J. H. Freed and W. L. Hubbell, *Biophys. J.*, 1999, 76, 3298-3306.
34. H. M. McConnell and W. L. Hubbell, *J. Am. Chem. Soc.*, 1971, 93, 314-326.

Combining EPR spectroscopy and X-ray crystallography to elucidate the structure and dynamics of conformationally constrained spin labels in T4 lysozyme single crystals

Philipp Consentius¹, Ulrich Gohlke², Bernhard Loll³, Claudia Alings³, Udo Heinemann^{2,1}, Markus C. Wahl^{3,5}, Thomas Risse^{1,4,*}

¹ Freie Universität Berlin, Institute of Chemistry and Biochemistry, Takustr. 3, 14195 Berlin, Germany

² Max Delbrück Center for Molecular Medicine in the Helmholtz Association, Robert-Rössle-Str. 10, 13125 Berlin, Germany

³ Freie Universität Berlin, Institute of Chemistry and Biochemistry, Laboratory of Structural Biochemistry, Takustr. 6, 14195 Berlin, Germany

⁴ Berlin Joint EPR Laboratory Freie Universität Berlin

⁵ Helmholtz-Zentrum Berlin für Materialien und Energie, Macromolecular Crystallography, Albert-Einstein-Straße 15, D-12489 Berlin, Germany

Supporting Information

Table S1. Crystallographic data collection and refinement statistics for T4 lysozyme 115/119RX determined at 298 K.

| | |
|--------------------------------|---------------------------------|
| PDB entry | 5NXO |
| Wavelength | 1.542 |
| Resolution range | 23.22 - 1.803 (1.868 - 1.803) |
| Space group | P 32 2 1 |
| Unit cell | 61.075 61.075 97.0657 90 90 120 |
| Total reflections | 35824 (2882) |
| Unique reflections | 19432 (1809) |
| Multiplicity | 1.8 (1.6) |
| Completeness (%) | 0.98 (0.92) |
| Mean I/sigma(I) | 13.92 (1.12) |
| Wilson B-factor | 25.52 |
| R-merge | 0.03501 (0.5192) |
| R-meas | 0.04951 (0.7342) |
| CC1/2 | 0.999 (0.625) |
| CC* | 1 (0.877) |
| Reflections used in refinement | 19430 (1812) |
| Reflections used for R-free | 956 (80) |
| R-work | 0.1696 (0.2710) |
| R-free | 0.2147 (0.3086) |
| CC(work) | 0.970 (0.722) |

| | |
|------------------------------|---------------|
| CC(free) | 0.941 (0.707) |
| Number of non-hydrogen atoms | 1434 |
| macromolecules | 1334 |
| Protein residues | 164 |
| RMS(bonds) | 0.019 |
| RMS(angles) | 1.88 |
| Ramachandran favored (%) | 98 |
| Ramachandran allowed (%) | 1.8 |
| Ramachandran outliers (%) | 0 |
| Rotamer outliers (%) | 0.71 |
| Clashscore | 1.48 |
| Average B-factor | 29.59 |
| macromolecules | 28.82 |
| solvent | 39.78 |

Statistics for the highest-resolution shell are shown in parentheses.

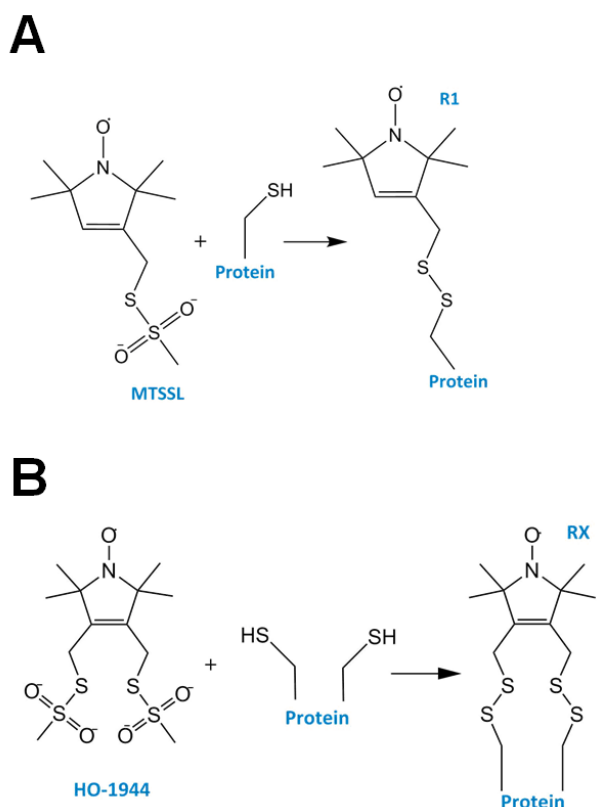


Figure S1. Schematic drawing of the labeling strategy. **(A)** Site-directed spin labeling of a single cysteine residue using the spin label 1-oxyl-2,2,5,5-tetramethyl- Δ 3-pyrroline-3-methyl (methanethiosulfonate, MTSSL) resulting in a covalent attachment via a disulfide bond. **(B)** Site-directed spin labeling of two adjacent cysteine residues using 2,2,5,5-tetramethyl-3,4-bis(sulfanylmethyl)-2,5-dihydro-1H-pyrrol-1-ol resulting in two covalent disulfide bonds.

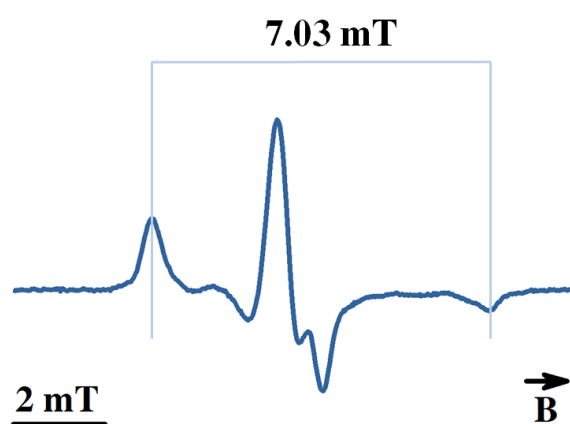


Figure S2. X-band EPR spectra of a homogenous suspension of crushed single crystals of T4L variant 118R1 performed at room temperature. The spectral width was determined to 7.03 mT.

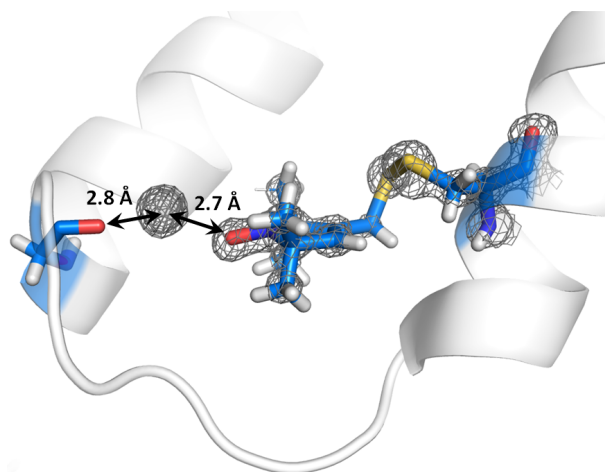


Figure S3. Stick-model of the side-chain modification L118R1 (PDB entry 5JDT) superimposed by a $2F_o-F_c$ difference electron density map contoured at 1.8σ (gray mesh).[4] Additional electron density corresponds to a water molecule, which facilitates hydrogen bonds between the oxygen atom of the nitroxide and the carbonyl moiety of residue G107.

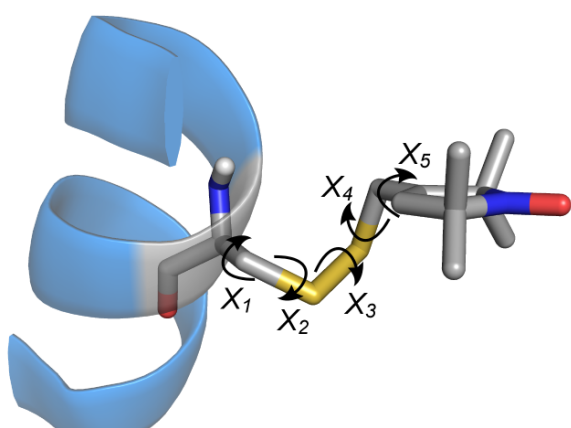


Figure S4. Stick-model of the chemical structure of the R1 side chain exemplarily attached to position 118C of T4 lysozyme. The internal dynamics of the R1 side chain commonly considered to be characterized by rotations around the five dihedral angles X_1 - X_5 .

Table S2. Static and dynamic parameters for EPR line-shape simulation based on the SLE.

| A_{xx} | A_{yy} | A_{zz} | g_{xx} | g_{yy} | g_{zz} | $\log R_{xx}$ | $\log R_{yy}$ | $\log R_{zz}$ | β_D | S | lw |
|------------|------------|----------|----------|----------|----------|---------------|---------------|---------------|-----------|------|------------|
| 0.62 mT | 0.59 mT | 3.7 mT | 2.0086 | 2.0068 | 2.0023 | 7.8- 8.2 | 7.8- 8.2 | 7.8- 8.2 | 0 | 0.91 | 0.17 mT |

Table S3. EPR fit parameters obtained using the effective Hamiltonian approach by fitting an X-band EPR spectrum of a homogenous suspension of crushed single crystals at room temperature. Best fit parameters are shown for T4L variant 118R1.

| Variant | A_{xx} [mT] | A_{yy} [mT] | A_{zz} [mT] | g_{xx} | g_{yy} | g_{zz} | Lw (FWHM) [mT] |
|---------|------------------|------------------|------------------|----------|----------|----------|----------------------|
| | | | | | | | |

| | | | | | | | |
|--------------|------|------|------|--------|--------|--------|------|
| 118R1 | 0.74 | 0.68 | 3.55 | 2.0084 | 2.0062 | 2.0023 | 0.25 |
|--------------|------|------|------|--------|--------|--------|------|

Table S4. EPR fit parameters obtained using the effective Hamiltonian approach by fitting an X-band EPR spectrum of a homogenous suspension of crushed single crystals at room temperature. Best fit parameters are shown for T4L variant 115/119RX.

| Variant | A_{xx} [mT] | A_{yy} [mT] | A_{zz} [mT] | g_{xx} | g_{yy} | g_{zz} | Lw (FWHM) [mT] |
|------------------|------------------|------------------|------------------|----------|----------|----------|----------------------|
| 115/119RX | 0.69 | 0.58 | 3.65 | 2.0084 | 2.0063 | 2.0023 | 0.20 |

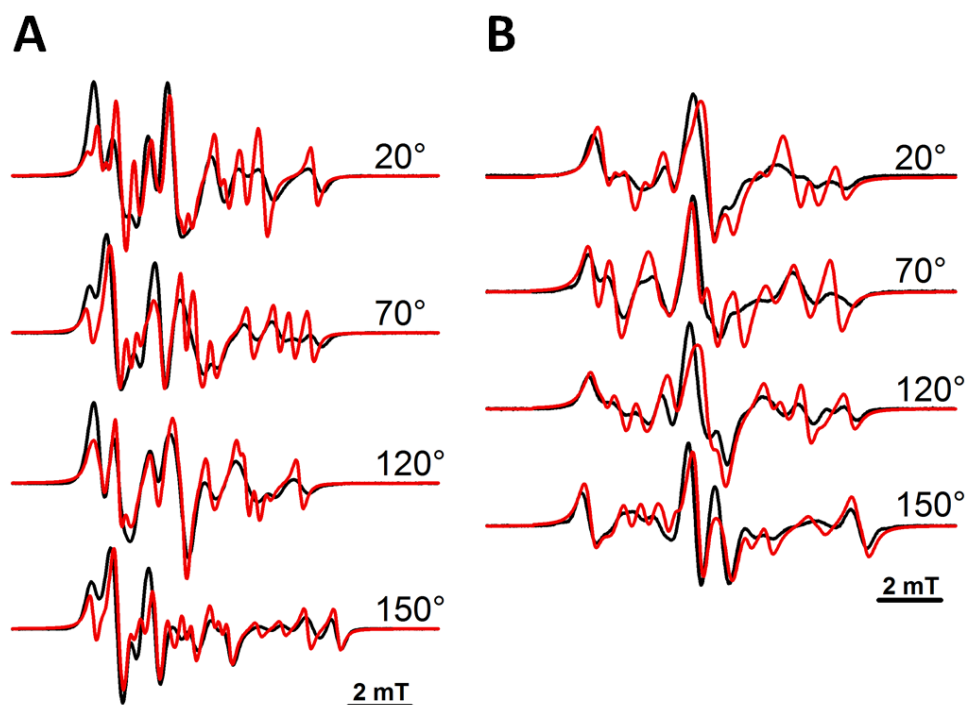


Figure S5. Four EPR Q-band (A) and X-band (B) spectra out of an angle dependent series taken for a single crystal of the T4L variant 118R1 (black traces). Angles are given with respect to a reference orientation (0°), for which the orientation of the unit cell was determined by X-ray crystallography. Red traces are simulations to the measured line shape using the effective Hamiltonian approach with principal components of the Zeeman- and hyperfine interactions as shown in **Table S3**.

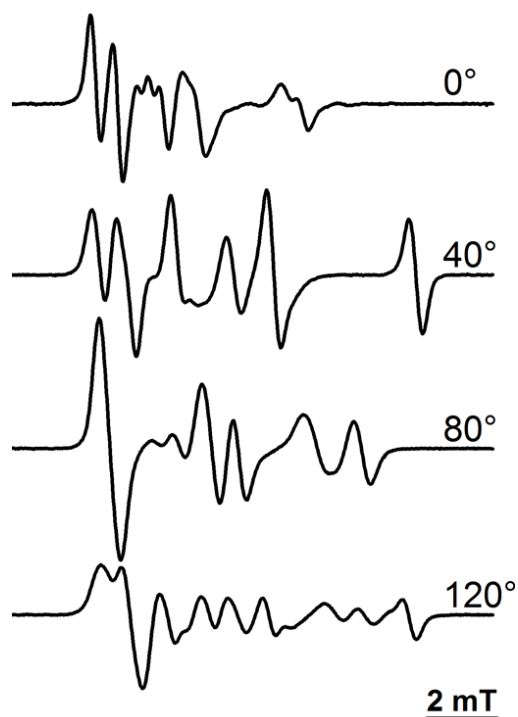


Figure S6. Four EPR Q-band spectra out of an angle dependent series taken from a single crystal of the T4L variant 115/119RX. Angles are given with respect to a reference orientation (0°), for which the orientation of the unit cell was determined by X-ray crystallography.

References

1. Adams, P.D., et al., *PHENIX: a comprehensive Python-based system for macromolecular structure solution*. Acta Cryst. D, 2010. **66**(Pt 2): p. 213-21.
2. Cruickshank, D.W., *Remarks about protein structure precision*. Acta Cryst. D, 1999. **55**(Pt 3): p. 583-601.
3. Chen, V.B., et al., *MolProbity: all-atom structure validation for macromolecular crystallography*. Acta Cryst. D, 2010. **66**(Pt 1): p. 12-21.
4. Consentius, P., et al., *Tracking transient conformational states of T4 lysozyme at room temperature combining X-ray crystallography and site-directed spin labeling*. J. Am. Chem. Soc., 2016. **138**(39): p. 12868-12875.
5. Matsumura, M. and B.W. Matthews, *Control of enzyme activity by an engineered disulfide bond*. Science, 1989. **243**(4892): p. 792-4.
6. Consentius, P., et al., *Internal dynamics of the 3-pyrroline-N-oxide ring in spin-labeled proteins*. J. Phys. Chem. Lett., 2017. **8**: p. 1113-1117.
7. Kabsch, W., *XDS*. In *International Tables for Crystallography*, A.E. Rossmann MG, Editor. 2006. p. pp 730-734.
8. Evans, P.R. and G.N. Murshudov, *How good are my data and what is the resolution?* Acta Cryst. D, 2013. **69**(Pt 7): p. 1204-14.
9. McCoy, A.J., et al., *Phaser crystallographic software*. J. Appl. Crystallogr., 2007. **40**(Pt 4): p. 658-674.
10. Winn, M.D., et al., *Overview of the CCP4 suite and current developments*. Acta Cryst. D, 2011. **67**(Pt 4): p. 235-42.

11. Emsley, P. and K. Cowtan, *Coot: model-building tools for molecular graphics*. Acta Cryst. D, 2004. **60**(Pt 12 Pt 1): p. 2126-32.
12. Bricogne, G.B., E Brandl, M Flensburg, C Keller, P Paciorek, W Roversi, P Sharff, A Smart, OS Vonrhein, C Womack, TO *BUSTER version 2.10.1*. . 2014, Global Phasing Ltd. : Cambridge, United Kingdom.
13. Schrödinger, L., *The PyMOL molecular graphics system, version 1.3 r1*. 2010. , 2010.
14. Hubbell, W.L. and McConnel.H.M., *Molecular Motion in Spin-Labeled Phospholipids and Membranes*. Journal of the American Chemical Society, 1971. **93**(2): p. 314-326.
15. Schneider, D.J., and J. H. Freed., *Calculating slow motional magnetic resonance spectra: a user's guide*, in *Spin Labeling Theory and Applications*, L.J.R. Berliner, J., Editor. 1989: New York, NY. p. 1–76.
16. Budil, D.E., et al., *Nonlinear-least-squares analysis of slow-motion EPR spectra in one and two dimensions using a modified Levenberg–Marquardt algorithm*. J. Magn. Reson., 1996. **120**(2): p. 155–189.
17. Stoll, S. and A. Schweiger, *EasySpin, a comprehensive software package for spectral simulation and analysis in EPR*. J. Magn. Reson., 2006. **178**(1): p. 42-55.